Corrections

BIOCHEMISTRY, MEDICAL SCIENCES. For the article "Structure of the topoisomerase II ATPase region and its mechanism of inhibition by the chemotherapeutic agent ICRF-187," by Scott Classen, Stephane Olland, and James M. Berger, which appeared in issue 19, September 16, 2003, of *Proc. Natl. Acad. Sci. USA* (**100,** 10629–10634; first published September 8, 2003; 10.1073/pnas.1832879100), the authors note that the recently published structure of the *Saccharomyces cerevisiae* topoisomerase II ATPase region bound to adenosine 5′-[β,γ-imino]triphosphate (ADPNP) and ICRF-187 contains an error. The drugs ICRF-187 and ICRF-186 are the respective (*S*)- and (*R*)-specific enantiomers of the racemic compound ICRF-159 (1, 2). During model building of our drug-inhibited complex, we relied on coordinates downloaded from the National Cancer Institute database for ICRF-187. We now have discovered that this file actually contains the ICRF-186 stereoisomer, and that the structure of the drug bound to topoisomerase II was correspondingly modeled incorrectly. Because the electron density for the ethanediyl linker region of the drug that contains the chiral center is poorly defined, the mistake was not immediately evident.

We have now rebuilt and refined the correct (*S*)-enantiomeric ICRF-187 compound into the ATPase region (see corrected Fig. 5 and legend below). Compared with the original model containing (*R*)-ICRF-186, the new model with (*S*)-ICRF-187 alters the angle at which the single methyl group extends from the chiral center of the linker. Despite this change, the well defined electron density of the two dioxopiperazine rings constrains the ethanediyl linker of ICRF-187 to adopt a slightly different twist than observed previously, shifting the coordinate position of the methyl substituent by only ≈0.5 Å. As a consequence, the methyl–pi interaction postulated to exist between the ICRF-187 ethanediyl linker and Tyr28 is maintained. Other interactions observed between the drug and topoisomerase II are similarly unaffected, and all discussions and conclusions of the paper still stand. Indeed, both ICRF-186 and ICRF-187 inhibit topoisomerase II with virtually the same K_i values (2–4), an observation that can be explained by the absence of stereospecific interactions between these drugs and the enzyme. The new coordinates have been deposited in the Protein Data Bank, www.rcsb.org (PDB ID code 1QZR).

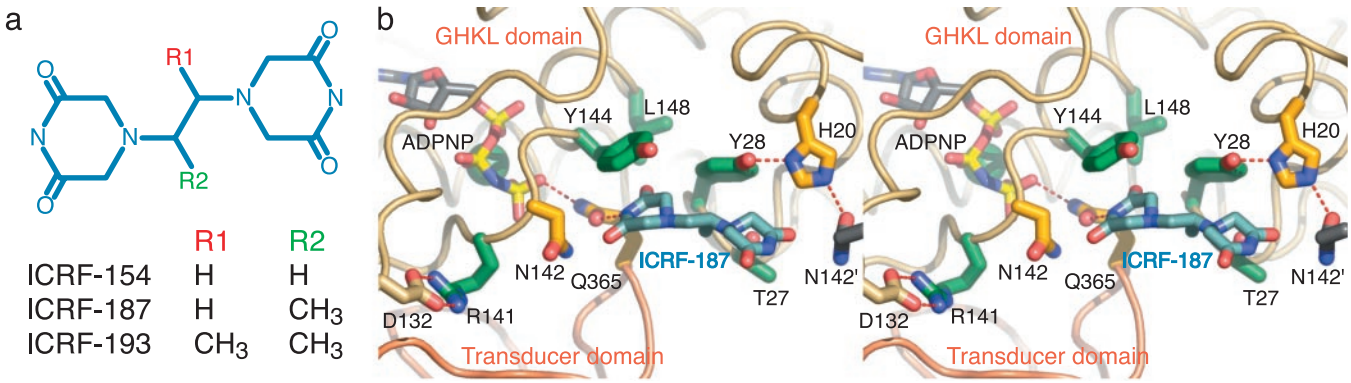

Fig. 5. Details of bisdioxopiperazine compounds and the ICRF-187-binding site. (*a*) Schematic of different bisdioxopiperazine compounds. (*b*) Stereo figure of drug-binding site (compare with Fig. 5 of the original paper). One protomer has been removed for clarity. ADPNP, ICRF-187, and residues within 5 Å of the drug are shown in stick representation and colored as in the original paper.

1. Hempel, A., Camerman, N. & Camerman, A. (1982) *J. Am. Chem. Soc.* **104,** 3453–3456.
2. Hasinoff, B. B., Kuschak, T. I., Yalowich, J. C. & Creighton, A. M. (1995) *Biochem. Pharmacol.* **50,** 953–958.
3. Hasinoff, B. B., Kuschak, T. I., Creighton, A. M., Fattman, C. L., Allan, W. P., Thampatty, P. & Yalowich, J. C. (1997) *Biochem. Pharmacol.* **53,** 1843–1853.
4. Snapka, R. M., Woo, S. H., Blokhin, A. V. & Witiak, D. T. (1996) *Biochem. Pharmacol.* **52,** 543–549.

www.pnas.org/cgi/doi/10.1073/pnas.2436153100

EVOLUTION. For the article "Active self-splicing group I introns in 23S rRNA genes of hyperthermophilic bacteria, derived from introns in eukaryotic organelles," by Camilla L. Nesbø and W. Ford Doolittle, which appeared in issue 19, September 16, 2003, of *Proc. Natl. Acad. Sci. USA* (**100,** 10806–10811; first published August 28, 2003; 10.1073/pnas.1434268100), the authors note that, due to an earlier misalignment, the position of the intron should be L1917, not L1926, and the intron should be annotated Tsu.bL1917 in Fig. 1*b*. The annotation of the sequence has been corrected in the GenBank database (accession no. AJ556793). Tsu.bL1917 is very similar in structure to two other introns in position L1917 (*Chlorosarcina brevispinosa*, GenBank accession no. L49150; and *Chaetosphaeridium globosum*, GenBank accession no. AF494279). The ORF in Tsu.bL1917 (i-Tsu1917b) clusters with the ORFs in these introns, as shown in Fig. 5, further supporting a recent transfer from a eukaryote.

www.pnas.org/cgi/doi/10.1073/pnas.2536363100

EVOLUTION. For the article "Synteny perturbations between wheat homoeologous chromosomes caused by locus duplications and deletions correlate with recombination rates," by Eduard D. Akhunov, Alina R. Akhunova, Anna M. Linkiewicz, Jorge Dubcovsky, David Hummel, Gerry Lazo, Shiaoman Chao, Olin D. Anderson, Jacques David, Lili Qi, Benjamin Echalier, Bikram S. Gill, Miftahudin, J. Perry Gustafson, Mauricio La Rota, Mark E. Sorrells, Deshui Zhang, Henry T. Nguyen, Venugopal Kalavacharla, Khwaja Hossain, Shahryar F. Kianian, Junhua Peng, Nora L. V. Lapitan, Emily J. Wennerlind, Vivienne Nduati, James A. Anderson, Deepak Sidhu, Kulvinder S. Gill, Patrick E. McGuire, Calvin O. Qualset, and Jan Dvorak, which appeared in issue 19, September 16, 2003, of *Proc. Natl. Acad. Sci. USA* (**100,** 10836–10841; first published September 5, 2003; 10.1073/pnas.1934431100), the author name Gerry Lazo should have appeared as Gerard R. Lazo. The online version has been corrected. The corrected author line appears below.

Eduard D. Akhunov, Alina R. Akhunova, Anna M. Linkiewicz, Jorge Dubcovsky, David Hummel, Gerard R. Lazo, Shiaoman Chao, Olin D. Anderson, Jacques David, Lili Qi, Benjamin Echalier, Bikram S. Gill, Miftahudin, J. Perry Gustafson, Mauricio La Rota, Mark E. Sorrells, Deshui Zhang, Henry T. Nguyen, Venugopal Kalavacharla, Khwaja Hossain, Shahryar F. Kianian, Junhua Peng, Nora L. V. Lapitan, Emily J. Wennerlind, Vivienne Nduati, James A. Anderson, Deepak Sidhu, Kulvinder S. Gill, Patrick E. McGuire, Calvin O. Qualset, and Jan Dvorak

www.pnas.org/cgi/doi/10.1073/pnas.2436097100

GENETICS. For the article "The presence of p53 mutations in human osteosarcomas correlates with high levels of genomic instability," by Michael Overholtzer, Pulivarthi H. Rao, Reyna Favis, Xin-Yan Lu, Michael B. Elowitz, Francis Barany, Marc Ladanyi, Richard Gorlick, and Arnold J. Levine, which appeared in issue 20, September 30, 2003, of *Proc. Natl. Acad. Sci. USA* (**100,** 11547–11552; first published September 12, 2003; 10.1073/pnas.1934852100), the authors note that several tumor samples in Table 1 were numbered incorrectly. OS17 should have read OS18, OS22 should have read OS24, OS27 should have read OS29, OS28 should have read OS30, and OS31 should have read OS33. This correction does not affect the conclusion that no tumors contain both a mutation of *p53* and an amplification of *HDM2*. The corrected table and its legend appear below.

Table 1. *p53* mutation screening

	Tumor	*p53* mutation	SSCP	PCR/LDR
1	OS2	Exon 8, D281H G → C	−	+
2	OS3	Exon 8, V272M G → A	−	+
3	OS6	Exon 5, R175H G → A	+	+
4	OS7	Exon 6, frameshift	+	NT
5	OS8	Exon 8, R273H G → A	−	+
6	OS11	Exon 5, frameshift, del 17nt	+	NT
7	OS18	Exon 6, E224D G → C	+	NT
8	OS19	Exon 6, Y220C A → G	+	NT
9	OS24	Exon 5, V173M G → A	+	NT
10	OS29	Exon 5, deletion codon 190	+	NT
11	OS30	Exon 5, V173G T → G	+	NT
12	OS33	Exon 8, R273C C → T	−	+

SSCP, single-strand conformation polymorphism; LDR, ligase-detection reaction; +, found by technique; −, not found; NT, not tested; det 17nt, deletion of 17 nucleotides.

www.pnas.org/cgi/doi/10.1073/pnas.2536673100

SPECIAL FEATURE, CHEMISTRY. For the article "Nutritional supplement chromium picolinate causes sterility and lethal mutations in *Drosophila melanogaster*," by Dion D. D. Hepburn, Jiarong Xiao, Sharell Bindom, John B. Vincent, and Janis O'Donnell, which appeared in issue 7, April 1, 2003, of *Proc. Natl. Acad. Sci. USA* (**100,** 3766–3771; first published March 20, 2003; 10.1073/pnas.0636646100), it should have been noted that the corresponding author, John B. Vincent, holds four patents dealing with isolated oligopeptides or synthetic chromium (III) complexes and their potential use as nutritional supplements or drugs. However, to date neither Dr. Vincent nor the University of Alabama has marketed or formed a company to market the chromium-containing species.

www.pnas.org/cgi/doi/10.1073/pnas.2536867100

Structure of the topoisomerase II ATPase region and its mechanism of inhibition by the chemotherapeutic agent ICRF-187

Scott Classen*, Stephane Olland†, and James M. Berger*‡

*Department of Molecular and Cell Biology, 237 Hildebrand Hall, University of California, Berkeley, CA 94720-3206; and †Wyeth Research, 85 Bolton Street, Cambridge, MA 02140

Edited by Nicholas R. Cozzarelli, University of California, Berkeley, CA, and approved July 11, 2003 (received for review June 3, 2003)

Type IIA topoisomerases both manage the topological state of chromosomal DNA and are the targets of a variety of clinical agents. Bisdioxopiperazines are anticancer agents that associate with ATP-bound eukaryotic topoisomerase II (topo II) and convert the enzyme into an inactive, salt-stable clamp around DNA. To better understand both topo II and bisdioxopiperazine function, we determined the structures of the adenosine 5′-[β,γ-imino]-triphosphate-bound yeast topo II ATPase region (*Sc*T2-ATPase) alone and complexed with the bisdioxopiperazine ICRF-187. The drug-free form of the protein is similar in overall fold to the equivalent region of bacterial gyrase but unexpectedly displays significant conformational differences. The ternary drug-bound complex reveals that ICRF-187 acts by an unusual mechanism of inhibition in which the drug does not compete for the ATP-binding pocket, but bridges and stabilizes a transient dimer interface between two ATPase protomers. Our data explain why bisdioxopiperazines target ATP-bound topo II, provide a structural rationale for the effects of certain drug-resistance mutations, and point to regions of bisdioxopiperazines that might be modified to improve or alter drug specificity.

Cell viability depends on the proper regulation of DNA topology. Because DNA is an extended double-helical polymer, events such as DNA replication, repair, and recombination naturally knot and entwine chromosomes. These entanglements become detrimental when daughter chromosomes partition into newly forming cells and can lead to chromosome breaks and cell death. Type IIA DNA topoisomerases (topos) enable cells to escape such fates by their ability to cleave a DNA duplex, pass a second DNA duplex through the break, and religate the cleaved DNA. This "DNA transport" reaction provides a physical means to disentangle entwined DNA duplexes and relieve torsional strain (reviewed in ref. 1).

Eukaryotic topo II is a homodimer with three distinct catalytic regions per subunit (Fig. 1*a*). A 400-aa N-terminal region has ATP-binding and hydrolysis activity. Two downstream regions of ≈300 and 450 residues (termed B′ and A′) together form a bipartite DNA-binding and cleavage domain. The overall sequence and organization of topo II are similar to those of two heterotetrameric bacterial enzymes, DNA gyrase and topo IV (2, 3). Together, these proteins constitute the type IIA topoisomerase superfamily.

A synthesis of biochemical and structural studies has led to a general model for type IIA topo function (4). DNA transport is initiated when the N-terminal ATPase region dimerizes in the presence of ATP (5–9). This event triggers a cascade of conformational changes that stimulate the B′A′ region to cleave and open a bound "gate" segment of DNA (G segment). If a "transport" segment of DNA (T segment) is captured by the ATPase domains upon dimerization, it is passed through the cleaved G segment, which is then closed and resealed. The T segment is thought to be expelled from the protein through a transient opening of the A′ dimer interface (10, 11).

While type IIA topos have long been of biophysical interest, these enzymes are also intensely studied by the biomedical community. Many antibiotics act on bacterial gyrase and topo IV (12), whereas a variety of anticancer drugs inhibit eukaryotic topo II (13). One such class of agents is the bisdioxopiperazines, which are used to ameliorate the cardiotoxic effects of anthracycline-based chemotherapies (14), and which are also in clinical trials for the treatment of leukemias and various solid tumors (15, 16). Glass-fiber filter and ultracentrifugation studies suggest that bisdioxopiperazines block topo II turnover by associating with and locking the ATPase region of the enzyme in its dimerized state (Fig. 1*b*) (17, 18).

To date, structural studies of type IIA topoisomerase/inhibitor complexes have focused on interactions between coumarin compounds and the bacterial enzyme, DNA gyrase (19–22). In contrast, a physical understanding of how drugs specifically recognize and inhibit eukaryotic topo II is still lacking. To better understand the action of the bisdioxopiperazine family of topo II inhibitors we determined the structure of the 45-kDa *S. cerevisiae* ATPase region (*Sc*T2-ATPase) bound to adenosine 5′-[β,γ-imino]triphosphate (ADPNP) both in the presence and in the absence of the bisdioxopiperazine ICRF-187 [(*S*)-4,4′-(1-methyl-1,2-ethanediyl)bis-2,6-piperazinedione]. Together, these structures show that a single bisdioxopiperazine molecule stabilizes a nucleotide-bound dimerized state of the ATPase regions by simultaneously binding to both protomers and bridging the dimer interface between subunits. These data explain why bisdioxopiperazines specifically inhibit the ATP-associated state of topo II and show how certain amino acid changes in the inhibitor-binding pocket lead to drug-resistant topo II enzymes.

Materials and Methods

Protein Purification. *Sc*T2-ATPase (residues 1–413 of *S. cerevisiae* topo II) was cloned into a modified pET28b plasmid containing a tobacco etch virus (TEV) protease cleavage site. Expression was carried out in *Escherichia coli* BL21-CodonPlus cells (Stratagene) to produce selenomethionine-labeled protein. Cells were grown at 37°C to an optical density of ≈0.8 at 600 nm and induced with 1 mM isopropyl β-D-thiogalactopyranoside (IPTG) for 6 h. Cells were harvested by centrifugation, subjected to freeze–thawing, and lysed by sonication in 20 mM Tris·HCl (pH 8.5)/250 mM KCl/10% (vol/vol) glycerol/2 mM 2-mercaptoethanol. Protein was purified over a Ni^{2+}-affinity column [Qia-

This paper was submitted directly (Track II) to the PNAS office.

Abbreviations: topo, DNA topoisomerase; ICRF-187, (*S*)-4,4′-(1-methyl-1,2-ethanediyl)bis-2,6-piperazinedione; ADPNP, adenosine 5′-[β,γ-imino]triphosphate; *Sc*T2-ATPase, *Saccharomyces cerevisiae* topo II ATPase region (residues 1–413); GyrB, DNA gyrase B subunit ATPase region.

Data deposition: The atomic coordinates and structure factors have been deposited in the Protein Data Bank, www.rcsb.org (PDB ID codes 1PVG and 1Q1D).

‡To whom correspondence should be addressed. E-mail: jmberger@uclink4.berkeley.edu.

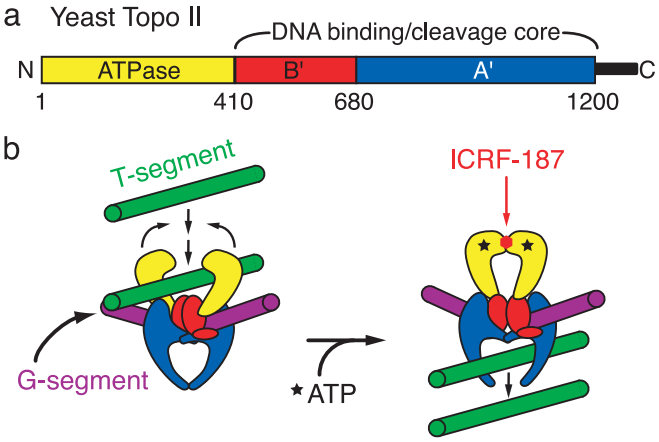

Fig. 1. (*a*) Domain organization of eukaryotic type IIA topoisomerases. Key functional modules of *Saccharomyces cerevisiae* topo II are labeled as follows: ATPase, yellow; B′, red; A′, blue; and a nonconserved C-terminal region, black. (*b*) Bisdioxopiperazine inhibition and the topo II reaction cycle. The enzyme normally transports one DNA segment through another in an ATP-dependent manner. Bisdioxopiperazines are thought to lock the ATPase regions in a nucleotide-bound dimeric state around double-stranded DNA, preventing the enzyme from resetting for subsequent rounds of strand passage.

gen Ni nitrilotriacetate (NTA) Superflow], digested with TEV protease at a 1:100 (wt/wt) ratio for 4 h at 20°C, then repassaged over a second Ni^{2+} column. Flow-through fractions from the second Ni^{2+} column containing *Sc*T2-ATPase were pooled, concentrated by ultrafiltration (Millipore Centriprep-30), and further purified by gel filtration over a Sephacryl-S300 column (Amersham Pharmacia). Peak fractions containing *Sc*T2-ATPase were reconcentrated to 12 mg/ml in 10 mM Tris·HCl (pH 7.5)/300 mM KCl/1 mM tris(2-carboxyethyl) phosphine for storage. Typical yields were 2.5 mg of protein per liter of culture.

Crystallization. Selenomethionine-labeled *Sc*T2-ATPase (12 mg/ml) was dialyzed against 5 mM Tris·HCl (pH 7.5)/100 mM KCl overnight at 4°C. Selenomethionine *Sc*T2-ATPase was crystallized by first adding 2 mM ADPNP and 5 mM $MgCl_2$ directly to the dialyzed protein stock and then mixing 1 μl of protein with 1 μl of crystallization buffer [50 mM sodium cacodylate (pH 6.5)/100 mM KCl/22% (wt/vol) PEG 1500/10% (vol/vol) glycerol] in microbatch format under paraffin oil at 20°C. Crystals (≈200 × 50 × 50 μm) appeared overnight and reached maximal size in 4–6 days, after which they were harvested in crystallization buffer plus 10% (vol/vol) ethylene glycol and flash frozen in liquid nitrogen. *Sc*T2-ATPase crystals with ICRF-187 were grown identically to the unbound crystals except that 5 mM ICRF-187 was added to the protein before adding ADPNP and $MgCl_2$. Crystals grown with ICRF-187 exhibited the same morphology as crystals grown with ADPNP alone.

Data Collection, Structure Determination, and Refinement. Data were collected at beamline 8.3.1 at the Advanced Light Source and processed with DENZO/SCALEPACK (23). Both drug-free and -bound crystal forms belong to the space group $P2_12_12_1$ with unit cell dimensions a = 58 Å, b = 71 Å, and c = 216 Å. There are two protomers per asymmetric unit for a solvent content of ≈50%. Heavy atom sites (11 selenium atoms per protomer) were determined for the ADPNP crystal form with SOLVE (24). Density modification of experimental maps and an initial C^{α} trace were performed with RESOLVE (24). Model building was carried out with O (25) and refinement with REFMAC5 (26) using TLS restraints (27). Waters were added with ARP/WARP (28). The ICRF-187-bound structure was solved by molecular replacement using the ADPNP-bound structure as a search model. Simulated anneal omit maps were used to ensure unbiased placement of bound ICRF-187. Surface representations were generated with GRASP (29) and all other figures were prepared with PYMOL (30).

Results

Structure of ATPase Domain from *S. cerevisiae* topo II. The *Sc*T2-ATPase/ADPNP structure was solved to 1.75-Å resolution by using multiwavelength anomalous dispersion (MAD). The final model contains residues 7–258, 276–334, and 340–406, and was refined to a working R factor of 20.6% and an R_{free} of 24.1% (Table 1, which is published as supporting information on the PNAS web site, www.pnas.org). There are only two outliers, Lys-243 in both monomers.

The *Sc*T2-ATPase protomer contains two domains (Fig. 2*a*). The first domain (residues 1–258) comprises a GHKL ATP-binding fold, an ATPase superfamily that includes diverse proteins such as gyrase B, Hsp90, CheA-type histidine kinases,

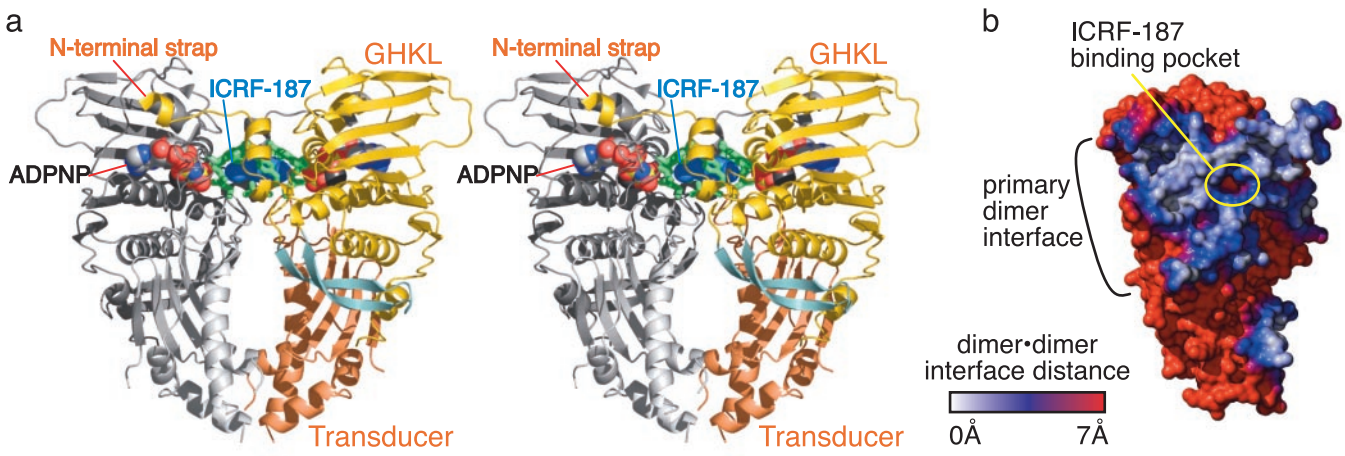

Fig. 2. (*a*) Stereo diagram of the *Sc*T2-ATPase dimer. The GHKL and transducer domains are colored gold and orange, respectively. A 22-aa β-hairpin unique to eukaryotic topo II is colored light blue. ICRF-187 is shown as blue spheres. All residues within 5 Å of the drug are colored green. ADPNP is shown as spheres and colored by atom. (*b*) Buried dimer surface area. This is a surface representation of a single protomer seen from the dimer interface, showing surfaces involved in dimer interactions. Distances between the surfaces of each protomer were calculated with GRASP (29) and range from 0 Å (white) to >7 Å (red). The ICRF-187-binding pocket sits in the middle of the primary dimer interface.

and MutL proteins (6, 31–34). This domain consists of an eight-stranded, antiparallel β-sheet backed by four α-helices. The second domain (residues 259–405) is formed by a four-stranded, mixed β-sheet with two α-helices, and is shared with a broad family of proteins including gyrase B, ribosomal protein S5, elongation factor G (EF-G), Hsp90, MutL, and RNase P (6, 32, 35–37). During the type II topo reaction, this domain is thought to transduce ATP-binding and hydrolysis signals to the downstream regions of the enzyme, coordinating DNA opening and transport events (6, 38, 39). This domain will henceforth be referred to as the transducer domain.

The *Sc*T2-ATPase region dimerizes upon nucleotide binding (5, 7, 9), forming a heart-shaped dimer ≈70 Å high and 65 Å wide (Fig. 2*a*). There are two dimer interfaces, which, together with the edges of the transducer domains, encompass a small hole ≈6 Å wide and 13 Å high. The primary dimer interface is formed between the GHKL domains and by two extended, N-terminal coil regions (the "straps") that each wrap around the local 2-fold symmetry axis to contact their dimer-related protomer. This interface is formed by residues 1–35, 104–147, and 360–376 of each protomer and buries ≈2,300 Å^2 of solvent-accessible surface area (Fig. 2*b*). The second dimer interface is smaller, burying ≈400 Å^2 of solvent-accessible surface area, and is formed by residues 340–348 of helix α11 and the β12–β13 connector loop.

The ATP-Binding Site. As anticipated from prior structures of the *E. coli* gyrase B subunit (GyrB) and MutL (6, 32), each topo II ATP-binding pocket is formed by portions of the GHKL and transducer domains of one protomer, and the N-terminal strap of the dimer-related protomer (Fig. 6, which is presented as supporting information on the PNAS web site). The largest contributions to the pocket arise from the GHKL domain. Three helices (α4–α6) and the β4–β5 connector loop form four sides of a box that surrounds the nucleotide. The floor of the box is composed of strands β4, β5, and β8, while an extended loop containing residues 123–144 forms a cover, termed the ATP-lid, that closes over the bound nucleotide. Specific contacts are made to the α- and β-phosphate groups of ADPNP by Asn-70/Lys-147 and Ser-127/Asn-129 of the GHKL domain. The γ-phosphate is hydrogen bonded by several backbone amides of the P-loop (residues 141–145) and Gln-365/Lys-367 of the transducer domain. A bound Mg^{2+} ion is octahedrally coordinated by a single nonbridging oxygen from each phosphate of the ADPNP, together with the carbonyl oxygen of Asn-70 and two water molecules. In addition, a water-mediated hydrogen bond to the N3 nitrogen of the adenosine base is formed by Tyr-12′ (where ′ denotes a dimer-related amino acid).

The ICRF-187-Binding Site. To define the interactions between topo II and bisdioxopiperazines, we determined the structure of a ternary *Sc*T2-ATPase·ADPNP·ICRF-187 complex. The structure was solved to 1.9-Å resolution by using molecular replacement and refined to a working *R* factor of 19.6% and an R_{free} of 23.7% (Table 1). A single drug molecule was observed to bind in a 350-Å^3 pocket formed at the primary dimer interface (Fig. 3*a*). The drug-binding pocket consists of 14 amino acids (7 from each protomer) from helices α2 and α3, and the C-terminal portion of the ATP-lid. The C-terminal transducer domain of the ATPase region also contributes a single amino acid, Gln-365, to the pocket. Superpositions of the ICRF-187-bound and -unbound structures show that the side chains of the 14 residues around the drug-binding site do not significantly change position upon drug binding (rms deviation = 0.302 Å over all atoms), and that the pocket is a preformed feature of the dimerized protein. However, six of the eight water molecules in the 350-Å^3 pocket are displaced upon association of *Sc*T2-ATPase with ICRF-187.

ICRF-187 is composed of two piperazinedione rings connected by a monomethyl-substituted ethanediyl linker (Fig. 3*b*). The most extensive ICRF-187/topoisomerase interactions occur through the two piperazinedione rings, which are surrounded by a "tyrosine-dome" whose ceiling and walls are formed by Tyr-144/Tyr-144′ and Tyr-28/Tyr-28′, respectively (Fig. 3). The tyrosines are buttressed by van der Waals contacts from Leu-148 and by hydrogen bonds from His-20/Asn-142′ to Tyr-28. Surprisingly, although ICRF-187 can potentially accommodate up to 12 hydrogen bonds, it forms only 2 with topo II: 1 between each of the cyclic *N*-acyl amides of the piperazinedione rings and the carbonyl oxygen of Gln-365 from each protomer (Fig. 3*b*). Subtraction of the van der Waals volume of ICRF-187 (225 Å^3) from the volume of the drug-binding cavity (350 Å^3) reveals two cavities above and below the plane of the drug with volumes of 35 and 95 Å^3, respectively (see Fig. 5). The larger of these contains the two water molecules that are not displaced by drug binding.

There is poor electron density for the methyl group extending from the ethanediyl linker of ICRF-187, suggesting either that it is disordered or that the drug is binding in two conformations. The best fit of the piperazinedione rings of ICRF-187 to the

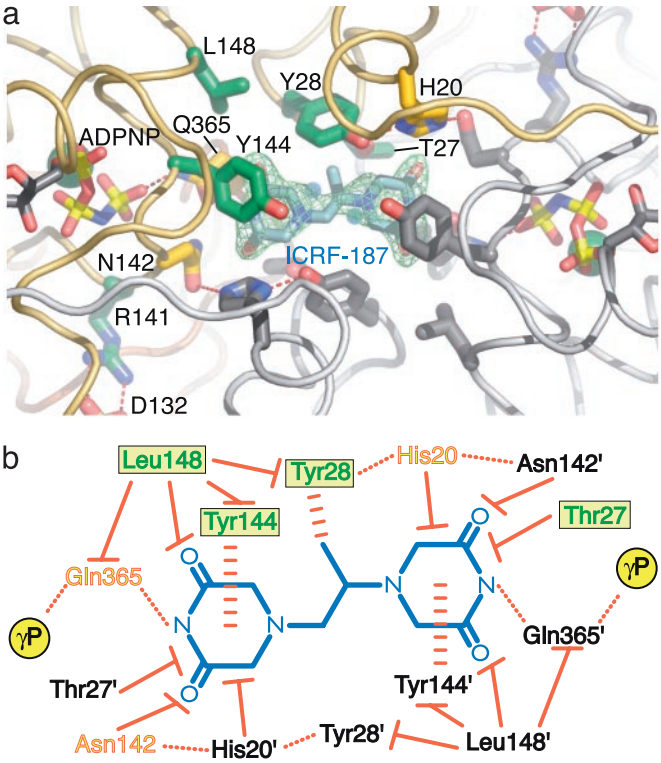

Fig. 3. ICRF-187-binding pocket and protein/drug interactions. (*a*) ICRF-187-binding pocket seen from the top of the dimer. An $F_{obs} - F_{calc}$ simulated-anneal omit electron density map shown in green is contoured at 1.5σ around ICRF-187. ADPNP, ICRF-187, and residues within 5 Å of the drug are shown in stick representation. For one protomer the residue positions correlated with drug resistance are colored dark green and other neighboring amino acids have been colored yellow. Residue side chains from the second protomer are colored gray. (*b*) Schematic diagram of protein/drug interactions. ICRF-187 is blue. Residues contacting the drug from each of the two protomers are indicated by colored or black text. For the colored protomer, the green residues in a yellow box indicate that drug-resistance mutations have been isolated at these positions. Orange/yellow residues are within 5 Å of ICRF-187 but have not yet been shown to affect drug efficacy when mutated. Hydrogen bonds are indicated by dotted red lines, stacking interactions are indicated by horizontally dashed red lines, and van der Waals interactions are indicated by solid red lines with a flat end. The γ-phosphates of bound ADPNPs are indicated by yellow circles.

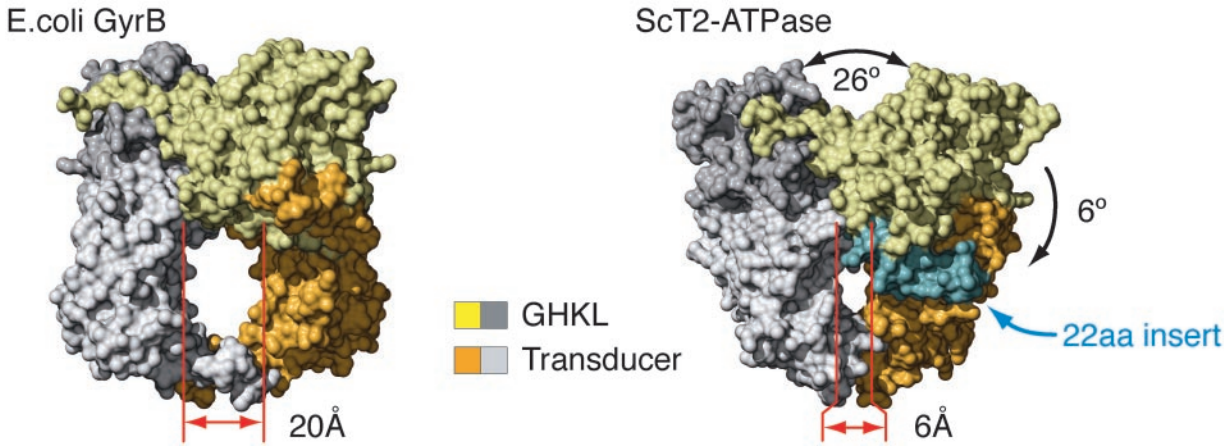

Fig. 4. Surface representation of *Sc*T2-ATPase and *E. coli* GyrB dimers. Each molecule has one protomer colored dark gray (GHKL) and light gray (transducer), and one protomer colored gold (GHKL) and orange (transducer). A 22-aa insert specific to eukaryotic topo II is colored light blue.

electron density orients the lone methyl group of the linker into the aromatic face of one of the two Tyr-28 residues, creating a potentially favorable methyl–π interaction between the drug and the amino acid. This unanticipated interaction may explain why three commonly used bisdioxopiperazine derivatives, ICRF-154, -187, and -193 demonstrate increasing potency as the number of methyl groups branching from their ethanediyl linkers increases from zero to two (40).

Discussion

Structural and Functional Comparisons of GyrB and *Sc*T2-ATPase. The ATPase regions of type IIA topos both regulate DNA cleavage and help capture a T-segment DNA for strand passage (1). Physical insights into this process were provided by the structure of an N-terminal 43-kDa fragment of GyrB (6), which showed that nucleotide binding dimerizes this region, forming a particle with an ≈20-Å hole in its center. The presence of this hole, which is seen in other gyrase structures (41, 42), has suggested that two ATPase protomers might directly associate with double-stranded DNA during enzyme turnover. Biochemical studies of gyrase have supported this proposal (43) but have also indicated that the interactions between this region of the enzyme and DNA are not as stable as might be expected if the ATPase segments were to fully encircle DNA (44, 45). ATPase and nitrocellulose filter-binding assays of the N-terminal domain of human topo IIα alone (residues 1–435) suggest that it has DNA-dependent ATPase activity (46) and is capable of binding DNA in an ATP/ADPNP-dependent manner (47), although similar studies with the *Sc*T2-ATPase fragment have not shown such effects (9).

The high degree of sequence homology between type IIA topos initially suggested that the structures of the eukaryotic and bacterial ATPase regions would be essentially identical. As expected, our data show that the overall folds of GHKL and transducer domains within the two enzyme superfamilies are indeed very similar (rms deviation = 1.475 and 1.817 Å, respectively). However, the interior hole of *Sc*T2-ATPase is much more constricted than seen for any prokaryotic GyrB structure (Fig. 4), measuring only 6 Å in diameter.

The narrow hole of the yeast protein arises from three factors. First, a slight interdomain rotation of ≈6° reorients the *Sc*T2-ATPase transducer domain further toward the dimer axis than in GyrB. Second, a 22-aa β-hairpin inserted between helices α3 and α4, which is unique to eukaryotic type IIA topos, partly occludes the upper half of the hole. Third, and most significantly, the orientation between the two GHKL domains is altered from that of GyrB such that each transducer domain swings inward, toward the local twofold dimer axis by about 13°, narrowing the ATPase hole by 14 Å (Fig. 4 and Fig. 7, which is published as supporting information on the PNAS web site). The architectures of the bisdioxopiperazine-binding pockets in the drug-free and -bound forms of the protein are identical, indicating that the observed conformation is a functional one populated by the dimerized protomer and targeted by the inhibitor. Moreover, we have observed an identical conformation in an alternate crystal form of *Sc*T2-ATPase with different crystal packing contacts (data not shown). Together, these observations suggest that the orientation of the GHKL domains and the small ATPase hole evident in the *Sc*T2-ATPase dimer reflect a natural configuration for this protein.

Although the small hole of the yeast ATPase region was unexpected, it is consistent with a unified mechanism for type IIA topoisomerase ATPase function that is parallel to that of bacterial gyrase. Indeed, although the 20-Å hole of GyrB could conceivably encompass a segment of double-stranded DNA, the fit would be snug at best. Given such observations, there are some useful implications for a tight or small ATPase hole in the type IIA topo reaction. One is that this feature may allow the enzyme to sense the presence of a T-segment DNA as the ATPase regions dimerize, perhaps generating physical strain that could be conformationally coupled to accelerate G-segment cleavage and opening. Another is that a small hole may prevent stable association of the ATPase regions with the T segment, which might otherwise impede T-segment transport.

Eukaryotic topo II and Bisdioxopiperazine Interactions. Prior biochemical and genetic data indicated that bisdioxopiperazines associate with a nucleotide-bound state of eukaryotic topo II, stabilizing a dimerized conformation of the ATPase regions and blocking enzyme turnover (9, 17, 48). Homology modeling studies using *E. coli* GyrB have supported this hypothesis, indicating that bisdioxopiperazine-resistance mutations cluster near the dimer interface (49–53, §). In addition, kinetic studies have shown that bisdioxopiperazines do not compete directly for the ATP-binding sites, but instead act noncompetitively at a stoichiometry of one drug molecule per topo II dimer (54).

Our work provides a structural rationale for these observations, showing that a single bisdioxopiperazine molecule prevents dissociation of the ATPase regions as a result of bridging the protein's dimer interface with its pseudo twofold symmetric

§Yalowich, J. C., Thampatty, P., Allan, W. P., Gee, G. & Hasinoff, B. B. (1998) *Proc. Am. Assoc. Cancer Res.* **39,** 375 (abstr.).

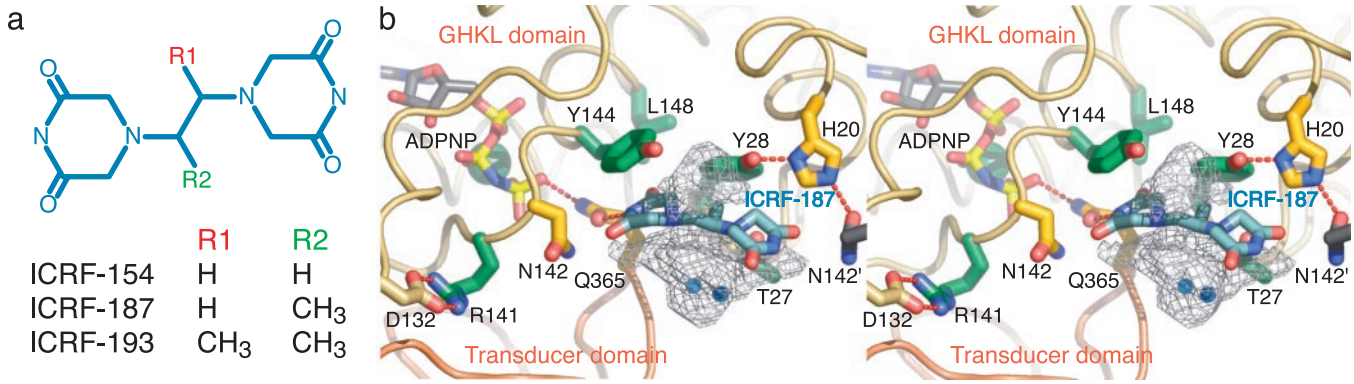

Fig. 5. Details of bisdioxopiperazine compounds and ICRF-187-binding site. (*a*) Schematic of different bisdioxopiperazine compounds. (*b*) Stereo figure of drug-binding site. One protomer has been removed for clarity. ADPNP, ICRF-187, and residues within 5 Å of the drug are shown in stick representation and colored as in Fig. 3. Subtraction of the van der Waals volume of ICRF-187 (225 Å^3) from the volume of the drug-binding cavity (350 Å^3) reveals two unfilled cavities above and below the plane of the drug (light gray mesh cages) with volumes of 35 and 95 Å^3, respectively.

structure. The details of the ICRF-187/topo II interactions explain many facets of drug action. First, bisdioxopiperazines bind to the N-terminal GHKL domains at a site distinct from ATP, a mode of inhibition that is very different from all other agents that target the type IIA topo ATPase regions by directly competing for nucleotide binding (20, 21, 42, 55, 56). Second, proper formation of each half of the drug-binding pocket depends on the positioning of the P-loop/ATP-lid by an associated nucleotide, explaining why the drug is specific for an ATP-bound intermediate of topo II. Finally, each piperazinedione ring of ICRF-187 hydrogen bonds to a key glutamine residue (Gln-365), which in turn hydrogen bonds to the γ-phosphate of bound ADPNP. This unanticipated interaction provides a physical link between bisdioxopiperazine binding and the catalytic center of ATP hydrolysis. Taken together, these findings help account for the hyperbolic mixed-type inhibition effects of bisdioxopiperazines on ATP hydrolysis and product release (9, 54).

Mechanisms of Bisdioxopiperazine Drug Resistance. To date, nine point mutations correlating with bisdioxopiperazine resistance have been isolated in eukaryotic type IIA topos (49–53, §). Five of these bisdioxopiperazine-resistance mutations map to the N-terminal ATPase region.

One of the first mutations isolated was derived from CHO cells selected for resistance to ICRF-187 and shown to contain a topo IIα allele with a Thr-48 → Ile alteration (57, §). In *S. cerevisiae* topo II, the equivalent residue, Thr-27, is part of the ICRF-187-binding site (Figs. 3 and 5). Thr-27 lies under the piperazinedione ring and contacts a carbonyl oxygen of ICRF-187 through van der Waals contacts. The Thr → Ile mutation introduces an extra methyl group into the drug-binding pocket and appears likely to disfavor drug binding by introducing unfavorable steric clashes. The effects of this mutation may be reflected in bacterial type IIA topos, which have a conserved methionine at this position and are refractory to bisdioxopiperazine inhibition (58).

A second bisdioxopiperazine-resistance mutation, Tyr-49 → Phe, was isolated from CHO cells selected for resistance to ICRF-159 (the racemate of ICRF-187) (49). Type IIA topos from CHO cells bearing this mutation also show different relative resistances to the bisdioxopiperazine compounds ICRF-154, ICRF-187, and ICRF-193 (Fig. 5*a*) (40, 49). Early attempts to understand the effects of the Tyr-49 → Phe mutation used homology modeling with the GyrB structure to suggest that an intermolecular hydrogen bond between this tyrosine and a histidine on the dimer-related protomer might stabilize the dimeric form of the ATPase region, and that disruption of this interaction would abrogate the ability of bisdioxopiperazines to generate the closed-clamp form of the enzyme (49). Our structure instead shows that in *S. cerevisiae* topo II, the equivalent amino acid (Tyr-28) actually forms an intraprotomer hydrogen bond to His-20, which in turn hydrogen bonds to Asn-142′ across the dimer interface (Figs. 3 and 5). Moreover, the aromatic face of Tyr-28 is positioned to directly interact with the methyl group of ICRF-187. The loss of the tyrosine···histidine hydrogen bond in the Tyr → Phe mutation may, therefore, have two effects on drug binding: (*i*) to destabilize an interaction important for proper dimerization of the ATPase domains and formation of the drug-binding site, and (*ii*) to weaken the walls of the drug-binding pocket by rendering the tyrosine less able to stably associate with the methyl groups of the bisdioxopiperazine ethanediyl linker.

A third mutation, Tyr-165 → Ser, was isolated from human NYH cells treated with ICRF-187 (51). The equivalent residue in *S. cerevisiae* is Tyr-144. *In vivo* clonogenic assays performed in *S. cerevisiae*, together with *in vitro* DNA decatenation assays, indicate that unlike other mutations, the Tyr-165 → Ser alteration is dominant (51). In the *Sc*T2-ATPase dimer, each Tyr-144 acts with its dimer-related partner to form part of the tyrosine dome over the piperazinedione rings of ICRF-187 (Figs. 3 and 5). The delocalized π electrons of the diacylamide moiety stack against the aromatic face of Tyr-144, forming the most extensive interactions between drug and protein. A Tyr → Ser mutation would completely remove this interaction and would be expected to severely destabilize drug binding.

A fourth mutation, Leu-169 → Phe, was isolated by two independent groups selecting for human topo IIα with resistance to ICRF-187 and ICRF-193 (52, 53). The equivalent position in *S. cerevisiae*, Leu-148, forms only modest van der Waals contacts with ICRF-187. However, Leu-148 packs between Tyr-28, Tyr-144, and the aliphatic portion of Gln-365, each of which extensively contacts ICRF-187 (Figs. 3 and 5). The introduction of a bulky phenylalanine at this position may crowd the adjacent tyrosine residues, both disrupting the local architecture of the tyrosine dome and perturbing the hydrogen bonds between the drug and Gln-365, therefore weakening protein/drug interactions.

A fifth mutation, Arg-162 → Gln, was isolated from human NYH cells treated with ICRF-187 (50). The equivalent residue in *S. cerevisiae* is Arg-141. Unlike other bisdioxopiperazine-resistance mutations, the Arg-162 → Gln mutation protects against etoposide-induced cytotoxicity when cells are treated with low doses of ICRF-187 (50). Additionally, the Arg-162 →

Gln mutant is the only bisdioxopiperazine-resistant mutant that is inhibited to the same degree as WT enzyme when exposed to ICRF-187 at saturating ATP concentrations (1 mM) *in vitro* (50). Consistent with these differences, Arg-162 does not interact directly with the drug. Instead, our structure indicates that the effect of the Arg → Gln mutation may arise indirectly through the enzyme's interaction with ATP. In the *Sc*T2-ATPase structure, Arg-141 lies within the ATP-lid, more than 7 Å away from ICRF-187. The backbone amide of Arg-141 hydrogen bonds to the γ-phosphate of the bound nucleotide while its guanidinium group forms a salt bridge to Asp-132 (Figs. 3 and 5). The Arg → Gln mutation would abrogate the salt bridge in the ATP-lid and appears likely to destabilize this region. Because two key residues that contribute to the drug-binding pocket are located in the ATP-lid (Asn-142 and Tyr-144), formation of a competent drug-binding pocket in the mutant probably can occur only when nucleotide concentrations are sufficiently high to drive proper configuration of the ATPase center and dimerization of two subunits.

Conclusions

The structures presented here of the ATPase region of eukaryotic topo II have allowed us to better understand the biophysical properties of topoisomerase mechanism and bisdioxopiperazine inhibition. The ADPNP-bound structure shows that the two halves of the ATPase dimer adopt a more constricted orientation than seen in bacterial gyrases, suggesting that DNA associations with this region might act as a steric trigger to regulate aspects of the topoisomerase reaction cycle. The ternary drug-bound complex reveals that bisdioxopiperazines inhibit topo II through an unusual mechanism in which the drug molecules do not compete for the ATP-binding pocket, but instead use their pseudo twofold symmetric structure to link the interface between two ATPase protomers. The structural information reported here explains many functional aspects of topo II/bisdioxopiperazine interactions, including the subtle interplay between ATP binding and drug inhibition, and the molecular basis of numerous drug-resistance mutations. This work also shows that two large cavities exist both above and below the plane of the drug and that several hydrogen bond donor/acceptor groups on side chains surrounding the drug-binding pocket remain unsatisfied (Fig. 5). Together, these data provide a striking example of how a small molecule can affect the conformational cycling of an enzyme by targeting protein–protein interaction surfaces as well as illuminate new directions for improving drug specificity and affinity.

We are grateful to James Holton at Beamline 8.3.1 of the Advanced Light Source for assistance with data acquisition. We thank Kevin Corbett for critical reading of the manuscript and members of the Berger Laboratory for helpful insights and discussion. We especially thank James Wang for early advice and directions on this project and John Nitiss for a sample of ICRF-187. S.C. gratefully acknowledges financial support from an American Cancer Society Postdoctoral Fellowship (PF-03-124-01-GMC) and J.M.B. acknowledges financial support from the National Institutes of Health (National Cancer Institute Grant CA77373).

1. Wang, J. C. (1998) *Q. Rev. Biophys.* **31,** 107–144.
2. Lynn, R., Giaever, G., Swanberg, S. L. & Wang, J. C. (1986) *Science* **233,** 647–649.
3. Peng, H. & Marians, K. J. (1993) *J. Biol. Chem.* **268,** 24481–24490.
4. Berger, J. M., Gamblin, S. J., Harrison, S. C. & Wang, J. C. (1996) *Nature* **379,** 225–232.
5. Osheroff, N. (1986) *J. Biol. Chem.* **261,** 9944–9950.
6. Wigley, D. B., Davies, G. J., Dodson, E. J., Maxwell, A. & Dodson, G. (1991) *Nature* **351,** 624–629.
7. Roca, J. & Wang, J. C. (1992) *Cell* **71,** 833–840.
8. Ali, J. A., Orphanides, G. & Maxwell, A. (1995) *Biochemistry* **34,** 9801–9808.
9. Olland, S. & Wang, J. C. (1999) *J. Biol. Chem.* **274,** 21688–21694.
10. Roca, J., Berger, J. M., Harrison, S. C. & Wang, J. C. (1996) *Proc. Natl. Acad. Sci. USA* **93,** 4057–4062.
11. Williams, N. L. & Maxwell, A. (1999) *Biochemistry* **38,** 13502–13511.
12. Levine, C., Hiasa, H. & Marians, K. J. (1998) *Biochim. Biophys. Acta* **1400,** 29–43.
13. Burden, D. A. & Osheroff, N. (1998) *Biochim. Biophys. Acta* **1400,** 139–154.
14. Keefe, D. L. (2001) *Semin. Oncol.* **28,** 2–7.
15. Von Hoff, D. D. (1998) *Semin. Oncol.* **25,** 31–36.
16. Budman, D. R., Calabro, A. & Kreis, W. (2001) *Leukemia* **15,** 1517–1520.
17. Roca, J., Ishida, R., Berger, J. M., Andoh, T. & Wang, J. C. (1994) *Proc. Natl. Acad. Sci. USA* **91,** 1781–1785.
18. Chang, S., Hu, T. & Hsieh, T. S. (1998) *J. Biol. Chem.* **273,** 19822–19828.
19. Lewis, R. J., Singh, O. M., Smith, C. V., Maxwell, A., Skarzynski, T., Wonacott, A. J. & Wigley, D. B. (1994) *J. Mol. Biol.* **241,** 128–130.
20. Lewis, R. J., Singh, O. M., Smith, C. V., Skarzynski, T., Maxwell, A., Wonacott, A. J. & Wigley, D. B. (1996) *EMBO J.* **15,** 1412–1420.
21. Tsai, F. T., Singh, O. M., Skarzynski, T., Wonacott, A. J., Weston, S., Tucker, A., Pauptit, R. A., Breeze, A. L., Poyser, J. P., O'Brien, R., *et al*. (1997) *Proteins* **28,** 41–52.
22. Lamour, V., Hoermann, L., Jeltsch, J. M., Oudet, P. & Moras, D. (2002) *Acta Crystallogr. D* **58,** 1376–1378.
23. Otwinowski, Z. & Minor, W. (1997) *Methods Enzymol.* **276,** 307–326.
24. Terwilliger, T. C. & Berendzen, J. (1999) *Acta Crystallogr. D* **55,** 849–861.
25. Jones, T. A., Zou, J. Y., Cowan, S. W. & Kjeldgaard, M. (1991) *Acta Crystallogr. A* **47,** 110–119.
26. Murshudov, G. N., Vagin, A. A., Lebedev, A., Wilson, K. S. & Dodson, E. J. (1999) *Acta Crystallogr. D* **55,** 247–255.
27. Winn, M. D., Isupov, M. N. & Murshudov, G. N. (2001) *Acta Crystallogr. D* **57,** 122–133.
28. Lamzin, V. S. & Wilsom, K. S. (1997) *Methods Enzymol.* **277,** 269–305.
29. Nicholls, A., Sharp, K. A. & Honig, B. (1991) *Proteins* **11,** 281–296.
30. DeLano, W. L. (2002) PYMOL (DeLano Scientific, San Carlos, CA).
31. Bergerat, A., de Massy, B., Gadelle, D., Varoutas, P. C., Nicolas, A. & Forterre, P. (1997) *Nature* **386,** 414–417.
32. Ban, C., Junop, M. & Yang, W. (1999) *Cell* **97,** 85–97.
33. Dutta, R. & Inouye, M. (2000) *Trends Biochem. Sci.* **25,** 24–28.
34. Bilwes, A. M., Quezada, C. M., Croal, L. R., Crane, B. R. & Simon, M. I. (2001) *Nat. Struct. Biol.* **8,** 353–360.
35. Murzin, A. G. (1995) *Nat. Struct. Biol.* **2,** 25–26.
36. Stams, T., Niranjanakumari, S., Fierke, C. A. & Christianson, D. W. (1998) *Science* **280,** 752–755.
37. Meyer, P., Prodromou, C., Hu, B., Vaughan, C., Roe, S. M., Panaretou, B., Piper, P. W. & Pearl, L. H. (2003) *Mol. Cell* **11,** 647–658.
38. Smith, C. V. & Maxwell, A. (1998) *Biochemistry* **37,** 9658–9667.
39. Corbett, K. D. & Berger, J. M. (2003) *EMBO J.* **22,** 151–163.
40. Hasinoff, B. B., Kuschak, T. I., Yalowich, J. C. & Creighton, A. M. (1995) *Biochem. Pharmacol.* **50,** 953–958.
41. Brino, L., Urzhumtsev, A., Mousli, M., Bronner, C., Mitschler, A., Oudet, P. & Moras, D. (2000) *J. Biol. Chem.* **275,** 9468–9475.
42. Lamour, V., Hoermann, L., Jeltsch, J. M., Oudet, P. & Moras, D. (2002) *J. Biol. Chem.* **277,** 18947–18953.
43. Tingey, A. P. & Maxwell, A. (1996) *Nucleic Acids Res.* **24,** 4868–4873.
44. Reece, R. J. & Maxwell, A. (1991) *Nucleic Acids Res.* **19,** 1399–1405.
45. Ali, J. A., Jackson, A. P., Howells, A. J. & Maxwell, A. (1993) *Biochemistry* **32,** 2717–2724.
46. Gardiner, L. P., Roper, D. I., Hammonds, T. R. & Maxwell, A. (1998) *Biochemistry* **37,** 16997–17004.
47. Campbell, S. & Maxwell, A. (2002) *J. Mol. Biol.* **320,** 171–188.
48. Hu, T., Sage, H. & Hsieh, T. S. (2002) *J. Biol. Chem.* **277,** 5944–5951.
49. Sehested, M., Wessel, I., Jensen, L. H., Holm, B., Oliveri, R. S., Kenwrick, S., Creighton, A. M., Nitiss, J. L. & Jensen, P. B. (1998) *Cancer Res.* **58,** 1460–1468.
50. Wessel, I., Jensen, L. H., Jensen, P. B., Falck, J., Rose, A., Roerth, M., Nitiss, J. L. & Sehested, M. (1999) *Cancer Res.* **59,** 3442–3450.
51. Wessel, I., Jensen, L. H., Renodon-Corniere, A., Sorensen, T. K., Nitiss, J. L., Jensen, P. B. & Sehested, M. (2002) *FEBS Lett.* **520,** 161–166.
52. Patel, S., Jazrawi, E., Creighton, A. M., Austin, C. A. & Fisher, L. M. (2000) *Mol. Pharmacol.* **58,** 560–568.
53. Jensen, L. H., Wessel, I., Moller, M., Nitiss, J. L., Sehested, M. & Jensen, P. B. (2000) *FEBS Lett.* **480,** 201–207.
54. Morris, S. K., Baird, C. L. & Lindsley, J. E. (2000) *J. Biol. Chem.* **275,** 2613–2618.
55. Sugino, A., Higgins, N. P., Brown, P. O., Peebles, C. L. & Cozzarelli, N. R. (1978) *Proc. Natl. Acad. Sci. USA* **75,** 4838–4842.
56. Leroy, D., Kajava, A. V., Frei, C. & Gasser, S. M. (2001) *Biochemistry* **40,** 1624–1634.
57. Hasinoff, B. B., Kuschak, T. I., Creighton, A. M., Fattman, C. L., Allan, W. P., Thampatty, P. & Yalowich, J. C. (1997) *Biochem. Pharmacol.* **53,** 1843–1853.
58. Sato, M., Ishida, R., Narita, T., Kato, J., Ikeda, H., Fukazawa, H. & Andoh, T. (1997) *Biochem. Pharmacol.* **54,** 545–550.